Pergamon

Int. Comm. Heat Mass Transfer, Vol. 23, No. 3, pp. 315–324, 1996

0735-1933/96 $12.00 + .00

PII S0735-1933(96)00017-6

SIMULATIONS OF SEDIMENTATION IN GLOBULITIC ALLOY SOLIDIFICATION

C. Beckermann and J. Ni
Department of Mechanical Engineering
The University of Iowa
Iowa City, IA 52242

(Communicated by J.P. Hartnett and W.J. Minkowycz)

ABSTRACT

Numerical simulations of the solidification of a binary metal alloy with a globulitic morphology are reported. The model is based on a previously developed two-phase approach that incorporates descriptions of the heat transfer, solute redistribution, melt convection, and solid transport on the system scale with microscopic models of nucleation, thermal and solutal undercoolings, grain growth and impingement. Results are obtained for solidification of an Al-4%Cu alloy in a rectangular cavity cooled from one side. Three simulations are conducted to investigate the effects of solid transport and nucleation rate on the final macrosegregation pattern and grain size distribution. It is shown that the nucleation rate has a profound influence on the settling behavior of the grains, which in turn leads to strong vertical variations in the composition and grain size.

Introduction

One of the most detrimental forms of macrosegregation and structural inhomogeneities in metal alloy castings is caused by the gravitationally induced floating or sedimentation of free solid in the form of dendrite fragments and equiaxed or globulitic grains. For example, the transport and sedimentation of small crystals is fundamental to the development and extent of the globulitic zone and the bottom cone of negative segregation observed in ingots [1]. Low-gravity experiments [2] have confirmed the important role of floating/settling of free solid in alloy solidification, but the results have remained qualitative and have not been supported by corresponding modeling studies. Whereas the modeling of thermal and solutal convection of the melt and the resulting macrosegregation during columnar solidification (i.e., with a stationary solid) has received considerable research attention in recent years [3], the study of transport phenomena during globulitic or equiaxed solidification has been neglected. Important additional issues that need to be

addressed in modeling of globulitic solidification are the origin and nucleation of the solid grains, their unconstrained growth in an undercooled melt, and their movement due to gravitational forces.

Considerable progress in modeling of equiaxed or globulitic metal alloy solidification has been made through the use of a so-called micro-macroscopic approach, that couples macroscopic heat flow calculations with microscopic models of nucleation, grain growth, and impingement [4-7]. However, these studies have neglected melt convection and solid transport. More recently, Ni and Beckermann [8] reported on a first attempt at modeling of globulitic alloy solidification in the presence of gravity-induced liquid and solid convection. The model used in this study is based on a two-phase approach for alloy solidification [9]. In this approach, the coupling between microscopic and macroscopic phenomena is achieved through (i) volume averaging of the microscopic transport equations and (ii) the use of separate conservation equations for the liquid and solid phases together with interfacial balances. In a similar manner as in the micro-macroscopic models [5], the model includes nucleation, thermal and solutal undercoolings at the growth front, and grain impingement. However, it is limited to alloys solidifying with a globulitic morphology in which the free grains are assumed to be spherical. While preliminary results of a single simulation were presented in Ni and Beckermann [8], this communication reports on an investigation of the effects of various nucleation rates and solid transport conditions on the final macrosegregation and grain size distribution.

Model Description

The system considered is illustrated in Fig. 1 and consists of a rectangular cavity (height H=0.1m, width L=0.05m) containing an Al-4%Cu alloy. The walls are impermeable and adiabatic, except for the left vertical wall which is cooled with a constant heat flux of 10^6 W/m^2. The alloy is

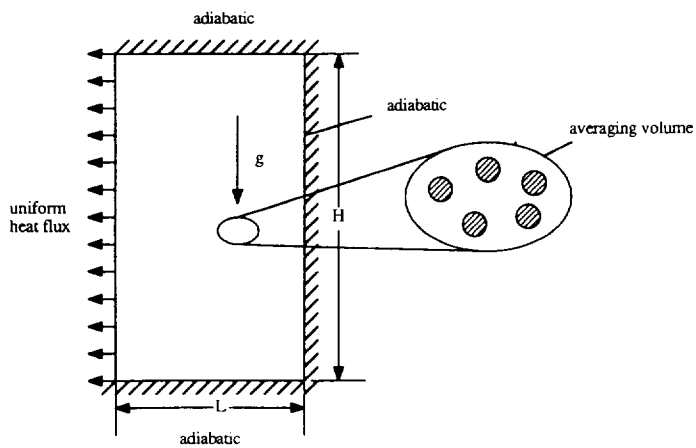

FIG. 1
Illustration of the physical system.

initially in the liquid state and quiescent at a uniform temperature (930 K) and concentration (0.04). All other conditions, as well as the properties, are identical to those listed in Tables 2 and 3 of Ni and Beckermann [8]. A detailed description of the two-phase model together with all governing equations can also be found in the above reference and is not repeated here for conciseness.

Of particular interest to the following discussion is the conservation equation used to calculate the grain density, n, [8-9]

$$\frac{\partial n}{\partial t} + \nabla\cdot(\mathbf{v}_S n) = \dot{n} \tag{1}$$

where $\mathbf{v}_S$ is the velocity of the solid phase (calculated from the momentum equation for the solid) and $\dot{n}$ is the net generation rate of grains per unit volume, which accounts for both the "birth" and "death" of grains. Equation (1) shows that the local grain density changes due to advection of grains in or out of a control volume and net generation of grains. The grains cease to move when the solid volume fraction approaches the maximum packing fraction (=0.637 for spheres). As in Ni and Beckermann [8], a most simple heterogeneous nucleation model is adopted for the generation of grains. Nucleation of new grains is assumed to occur instantaneously at the liquidus temperature. The initial grain diameter, d_{Si}, is taken to be 10^{-6} m. The instantaneous nucleation concept is described in detail by Stefanescu et al. [6]. The nucleation rate is taken to be a constant (either 10^{11} l/m^{3}s or 10^9 l/m^{3}s; see below), i.e., it is not a function of the local cooling rate (as in [6]). Nucleation can only take place if the local grain density before nucleation is equal to zero, implying that no new grains will nucleate in the immediate neighborhood of existing grains. The latter assumption is necessary in view of the fact that the present two-phase model considers only a single grain size in a given averaging volume. Death of grains occurs if grains are advected into regions of higher temperature and remelt to a diameter below the initial one. Then, the local grain density is instantaneously reset to zero. Thus, grains may exist in regions of superheated melt as long as their diameter is above the initial diameter. It also follows that no grains will die if the local temperature is below the liquidus temperature. It should be noted that future, more sophisticated, nucleation models can be incorporated without difficulty.

With the knowledge of the grain density, n, and the assumption of spherical grains, the local grain radius, R_S, can be calculated from

$$R_S = \left[\frac{3\varepsilon_S}{4\pi n} \right]^{\frac{1}{3}} \tag{2}$$

where ε_s is the solid volume fraction which, in turn, depends on the solid velocity and the solidification rate (see [8]). Equation (2) also allows for the calculation of the final grain size distribution in the fully solidified cavity (i.e., when $\varepsilon_S = 1$).

Numerical Procedures

The model equations were solved using the PHOENICS computer code, which is one of the few commercially available codes having a built-in two-phase capability. All constitutive, property, and interfacial relations can be programmed in user-accessible subroutines. The conservation equation for the grain density, Eq. (1), was discretized separately using the upwind scheme in a manner consistent with the discretization scheme employed in PHOENICS for the other conservation equations. All other details can be found in Ni [10] and Ni and Beckermann [11].

A grid system of 25x25 nodal points was utilized for the calculations presented in this paper. The grid was slightly skewed towards the domain boundaries. Trial calculations showed that the grid system represents a reasonable compromise between accuracy and computational time. The time step was reduced until time step independent results were obtained. The numerical code was carefully checked and validated for several limiting cases, such as solidification without liquid convection and solid transport, and sedimentation of spheres without solidification [7,10]. The calculations were performed on a IBM 3090 computer and required approximately 2000 CPU seconds for one second of simulation time.

Results and Discussion

Three simulations were performed to illustrate the effects of nucleation and solid transport on the solidification process and the final solid properties. In the first simulation (1), the solid velocity was artificially forced to zero everywhere, still allowing for thermosolutal natural convection of the melt in the pure liquid region and the now stationary mushy zone. The nucleation rate, $\dot{n}$, was 10^{11} l/m^{3}s, controlling the grain size in the mushy zone. The second (2) and third (3) simulations featured both liquid and solid movement, according to the full two-phase model. The only difference between the two simulations was that the second simulation had a nucleation rate of 10^{11} l/m^{3}s, whereas in the third simulation $\dot{n} = 10^9$ l/m^{3}s.

Simulation 1

Selected results for Simulation 1 are provided in Fig. 2. Figures 2a to 2d show the liquid velocity vectors superimposed on the solid fraction, ε_S, isopleths at 10s, 30s, 50s, and 70s, respectively. All isopleths are plotted in equal increments. Solidification proceeds in an almost one-dimensional fashion from the left wall, as is evident from the vertical and straight solid fraction isopleths, with the mushy zone sandwiched between pure solid and liquid regions. This indicates

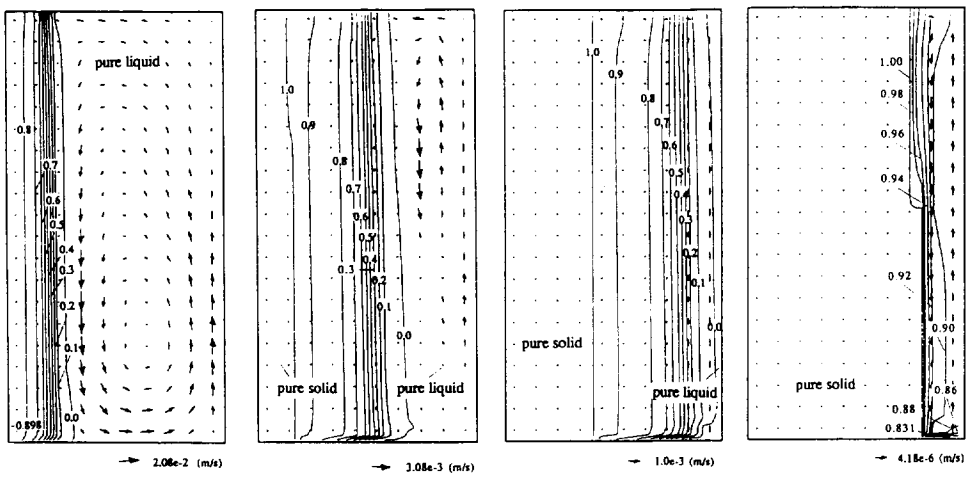

(a) 10s (b) 30s (c) 50s (d) 70s

FIG. 2
Liquid velocity vectors and solid volume fraction contours for Simulation 1 (stationary solid, $\dot{n}=10^{11}$ l/m^{3}s).

that the natural convection melt flow has little effect on the heat transfer. The flow generally consists of a counterclockwise rotating convection cell. In the present system, the thermal and solutal buoyancy forces near the mushy zone/liquid region interface are augmenting each other. The thermal buoyancy force acts downward because of the cooling at the left wall. The solutal buoyancy force points also downward because the rejected copper-rich interdendritic liquid has a larger density than the liquid of the original composition away from the mushy zone. Note that the scale of the liquid velocities drastically decreases at later times, as the pure liquid region diminishes in size and more of the melt flow takes place in the mushy zone. This is because of the large interfacial drag offered by the intergranular flow channels in the porous, rigid mushy zone. Maximum velocities in the mushy zone range from 10^{-3} to 10^{-4} m/s. The resulting macrosegregation pattern is discussed below.

Simulation 2

Corresponding results of Simulation 2, including liquid convection and solid transport (with $\dot{n}=10^{11}$ l/m^{3}s), are shown in Fig. 3. At 10s (Fig. 3a) the maximum solid fraction occurs along the lower third of the cooled wall, where the globulitic crystals have packed and the velocities are small. On the other hand, the solid fraction along the upper third of the cooled wall is small, indicating that the crystals are advected downwards. In fact, a considerable amount of solid is present near the lower (adiabatic) wall of the enclosure. Again, the liquid flow consists of a

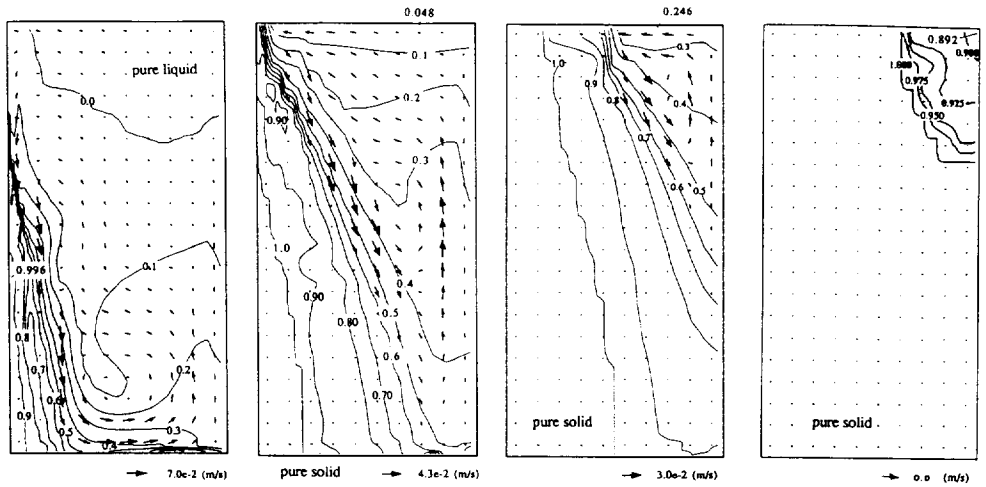

(a) 10s (b) 30s (c) 50s (d) 70s

FIG. 3
Liquid velocity vectors and solid volume fraction contours for Simulation 2 (moving solid, $\dot{n}=10^{11}$l/m^{3}s).

counterclockwise rotating convection cell. The liquid advects crystals to the right portion of the enclosure where the melt is still of the original composition and near the liquidus temperature. A pure liquid region ($\varepsilon_S=0$) only exists in the upper-right portion of the enclosure. The pure liquid region can be directly attributed to the sedimentation of grains. For a solid fraction greater than about 0.6, the grains have packed and do not move. This can be observed along the lower portion of the cooled wall, where the liquid percolates downward through the stationary bed of globulitic grains. These velocities cannot be seen in Fig. 3a due to the large velocity scale used in this figure. In the lower-left corner, the solid fraction is so large that all velocities vanish.

At 30s (Fig. 3b), solidification has progressed considerably. A pure solid region exists near the lower portion of the cooled wall, indicating that the temperature at these locations has fallen below the eutectic temperature. Virtually the entire enclosure is occupied by either stationary ($\varepsilon_S>0.637$) or moving ($\varepsilon_S<0.637$) globulitic grains. An accumulation of sedimented crystals can be observed at the lower wall. However, some solid is advected with the liquid to the right and upper portions of the enclosure into regions of higher temperature, where they partially remelt [8]. At 50s and 70s (Figs. 3c and 3d), the overall transport phenomena are similar as at 30s, with the fully solidified region growing at the expense of the convecting two-phase region. Even at 50s, the uppermost portion of the cooled wall is relatively free of solid, which can be attributed to the downward flow of melt and grains along the cooled wall. As expected, the upper right corner is the last region to solidify. Note that the magnitude of the velocities continually decreases. A more complete

discussion of Simulation 2, together with plots of the temperature and concentration field evolutions, can be found in Ni and Beckermann [8].

Simulation 3

Intermediate results of Simulation 3 are presented in Fig. 4. In Simulation 3, the nucleation rate was only 10^9 l/m^{3}s, as opposed to 10^{11} l/m^{3}s for Simulation 2, resulting in a lower grain density and, hence, a larger grain diameter at the same solid fraction. This exerts a major influence on the settling characteristics of the solid grains, since the relative velocities between the solid and liquid phases can be expected to be much larger due to the reduced interfacial drag, when compared to Simulation 2. As can be seen from Fig. 4, the different settling behavior has a profound effect on the solid fraction distribution during the solidification process. At 10s (Fig. 4a), there already exists a layer of sedimented grains at the bottom wall, which nucleated near the cooled left vertical wall and grew during their downward motion through undercooled melt. The solid fraction along the cooled wall is extremely low, indicating that the grains do not adhere to the vertical surface. Only small grains are advected with the counterclockwise rotating melt up along the right wall. Once they reach superheated melt in the upper right portion of the cavity, the grains partially remelt. At 30s (Fig. 4b), a packed bed of globulitic grains having a triangular shape can be observed in the lower right corner. Now, a relatively thin layer of attached solid starts to develop from the bottom on the cooled left wall. Figures 4c (50s) and 4d (70s) show that the grains continue to settle on the bottom layer, resulting in a virtually horizontal interface between the

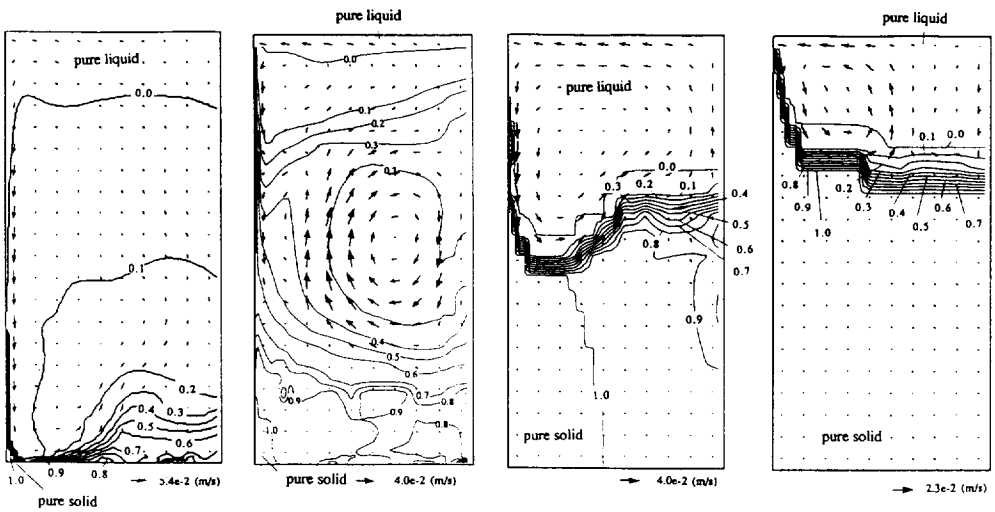

(a) 10s (b) 30s (c) 50s (d) 70s

FIG. 4
Liquid velocity vectors and solid volume fraction contours for Simulation 3 (moving solid, $\dot{n} = 10^9$l/m^{3}s).

packed bed of grains and the pure liquid region. Except for the thin layer of attached solid on the left cooled wall, it appears as if solidification proceeds in a relatively one-dimensional fashion from the bottom, despite the fact that the bottom surface is adiabatic. This behavior is in strong contrast with the almost vertical growth front for Simulation 1 (see Fig. 2) where the grains are stationary from the beginning. Furthermore, Simulation 3 is characterized by an almost solid-free melt region above the packed bed of sedimented grains (see Figs. 4c and 4d), whereas in Simulation 2 there exist much higher solid fractions in the upper portions of the cavity (see Fig. 3). Again, this can be attributed to the higher interfacial drag in Simulation 2, causing grains to be advected by the melt throughout the cavity. In fact, comparing Figs. 4a/b and 4c/d, the upper half of the cavity "clears" as solidification proceeds and the grains increase in size.

Comparison of Macrosegregation Patterns

Figures 5a, 5b, and 5c show the final macrosegregation patterns for the three simulations. The same concentration scale is used in each of the three plots to allow for a direct comparison. Figure 5a shows that for Simulation 1 (stationary solid), the downward flow of solute-rich melt through the mushy zone during solidification causes the bottom portion of the cavity to be positively segregated at the expense of the top portion. This is in strong contrast with the macrosegregation patterns for the simulations with grain transport. In particular, Fig. 5c for Simulation 3 shows large positive segregation in the upper portion of the cavity, while the lower two-thirds are negatively segregated. This can be directly attributed to the sedimentation of solute-poor grains during solidification. In the uppermost part of the cavity, the continual settling of

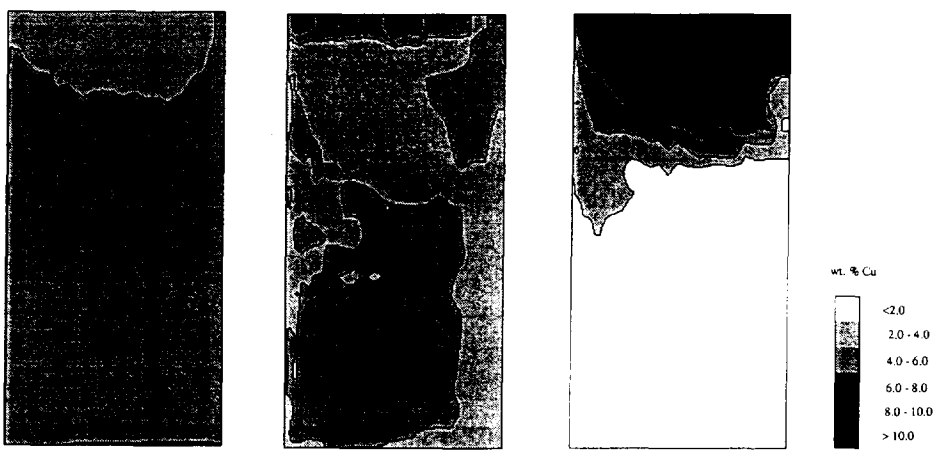

(a) Simulation 1 (max.=7.6% Cu, min.=3.5% Cu)

(b) Simulation 2 (max.=8.5% Cu, min.=2.5% Cu)

(c) Simulation 3 (max.=32.2% Cu, min.=1.0% Cu)

FIG. 5
Comparison of final macrosegregation patterns.

grains causes a stationary solid structure to form only when the temperature is already close to the eutectic value, resulting in a maximum concentration of 32.2%Cu (the eutectic concentration being 32.7%Cu). Figure 5b for Simulation 2 shows features from both Simulations 1 and 3. The much more uniform final composition, compared to Simulation 3, can be explained by the more dispersed and co-current flow of the solid and liquid phases, indicating that a finer grain structure results in less macrosegregation.

Final Grain Size Distributions

Figures 6a and 6b show the final grain radius distributions, as calculated from Eq. (2) with ε_s=1, for the two simulations with grain transport. In Simulation 1, the grain density, n, remains uniform, because the grains are stationary [v_S=0 in Eq. (1)] and the nucleation rate, $\dot{n}$, was constant. Therefore, any nonuniformities in the final grain size distributions in Fig. 6 (Simulations 2 and 3) can be attributed to grain transport. Note that Eq. (2) does not take into account possible variations in the grain size due to different amounts of eutectic present, but merely reflects variations in the grain density, n. According to Eq. (2) (with ε_s=1), grain desnsities of 10^{11} and 10^9 1/m^3 result in final grain radii of 134 and 620 μm, respectively.

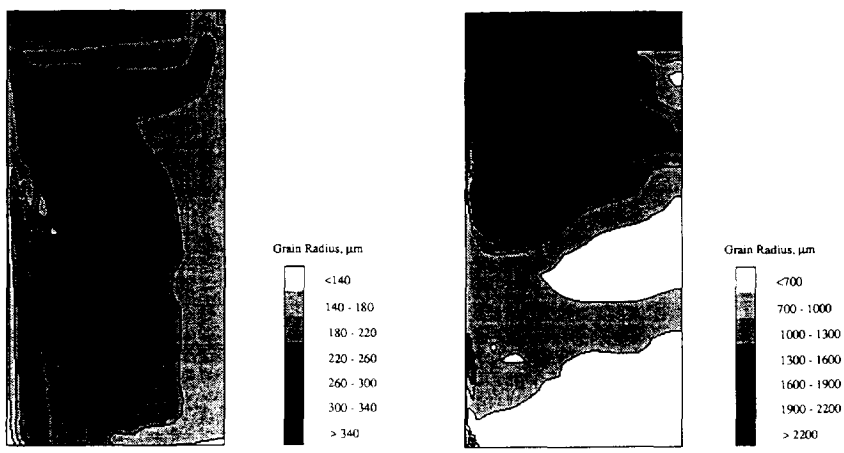

(a) Simulation 2 (b) Simulation 3

FIG. 6
Comparison of final grain radius distributions.

Figure 6a shows that in Simulation 2 relatively small grains are predicted in a small layer adjacent to the lower portion of the cooled left wall and near the lower right corner of the cavity. The corresponding high grain density is due to the advection and settling of grains into these regions. Larger grains can be observed in the upper portion of the cavity and in a band next to the layer of fine grains along the lower left wall. The effect of grain settling on the final grain size distribution is even more pronounced in Simulation 3 (Fig. 6b). The grain radius drastically

increases towards the top of the cavity as a result of the downward movement of the grains. Similar observations have been made in the experiments of McCartney and Ahmady [11].

Conclusions

A two-phase model was used to predict transport phenomena during globulitic solidification of a binary metal alloy. The model incorporates nucleation, thermal and solutal undercooling, and interfacial drag together with heat transfer, solute redistribution, melt convection, and solid transport on the system scale. The results reveal the effects of thermosolutal convection and sedimentation on the evolution of macrosegregation and the final grain size distribution. In particular, the nucleation rate is seen to have a profound influence on the grain transport and the final patterns. It certainly appears to be questionable to expect a one-to-one correspondence between the local grain size observed in a solidified casting and the nucleation and cooling rates at the same location, as is commonly done in the literature [4-6]. Nonetheless, the present study brings us no closer to developing a more realistic nucleation model. Fragmentation of dendrites and agglomeration are just a few of the many issues that need to be addressed in a nucleation model that is valid in the presence of convection. In addition, extension of the model to dendritic growth and experimental validation are important future research issues.

Acknowledgments

The authors would like to acknowledge financial support from the National Science Foundation under grants CBT-8808888 and CTS-8957149, the National Aeronautics and Space Administration under Grant No. NCC3-290, and by the ALCOA Technical Center. Computer facilities were made available by the University of Iowa WEEG Computing Center.

References

1. M.C. Flemings, *Solidification Processing*, McGraw-Hill, New York (1974).
2. M.H. Johnston and R.A. Parr, in *Materials Processing in the Reduced Gravity Environment of Space* (Edited by G.E. Rindone), pp. 651, Materials Research Society, (1982).
3. F.P. Incropera and R. Viskanta, presented at *Oji International Seminar on Advanced Heat Transfer in Manufacturing and Processing of New Materials*, Tomakomai, Hokkaido, Japan, October 28-31 (1990).
4. Ph. Thevoz, J.L. Desbiolles and M. Rappaz, Metall. Trans. A, *20A*, pp. 311 (1989).
5. M. Rappaz, Int. Materials Reviews, *34*, pp. 93 (1989).
6. D.M. Stefanescu, G. Upadhya and D. Bandyopadhyay, Metall. Trans. A, *21A*, pp. 997 (1990).
7. R.J. Feller and C. Beckermann, International Communications in Heat & Mass Transfer, *20*, pp. 311 (1993).
8. J. Ni and C. Beckermann, J. Materials Processing and Manufacturing Science, *2*, pp. 217 (1993).
9. J. Ni and C. Beckermann, Metall. Trans. B, *22B*, pp. 349 (1991).
10. J. Ni , *Ph.D. Thesis*, The University of Iowa, Iowa City, IA (1991).
11. D.G. McCartney and S.M. Ahmady, Metall. Mat. Trans., *25A*, pp. 1097 (1994).

Received September 22, 1995